Available online at www.sciencedirect.com
ScienceDirect
NDT&E International 40 (2007) 158–167
NDT&E international
www.elsevier.com/locate/ndteint

Case depth determination in heat-treated industrial steel products using photothermal radiometric interferometric phase minima

Chinhua Wang[a,b,*], Andreas Mandelis[a]

[a]Department of Mechanical and Industrial Engineering, Center for Advanced Diffusion-Wave Technologies, University of Toronto, Toronto, Ont., Canada M5S 3G8
[b]Institute of Modern Optical Technologies, Suzhou University, 1 Shizi Street, Suzhou, Jiangsu Province 215006, PR China

Received 17 May 2006; received in revised form 9 August 2006; accepted 1 September 2006
Available online 27 October 2006

Abstract

A quantitative calibrated methodology based on photothermal radiometric (PTR) depth-profilometry for non-contact, non-intrusive determination of effective case depth in heat-treated case-hardened steel products was developed. Several types of heat-treated C1018 industrial steel screw products (with hexagonal, cylindrical and spherical heads) are statistically evaluated using the case-depth-induced interferometric thermal-wave phase minima. Calibration curves for each type of sample are established with the help of conventional destructive indenter measurements. It is shown that PTR thermal-wave interferometric phase minima can be used as a fast, on-line inspection methodology of industrial steel products for non-destructive quality and feedback control of heat-treating processes.
© 2006 Elsevier Ltd. All rights reserved.

Keywords: Heat-treated steel; Case depth; Photothermal radiometry; Non-destructive inspection; Swept-sine cross-correlation; Calibration; Lock-in amplifier

1. Introduction

Hardness and case depth measurements are the most important parameters for the quality monitoring of case-hardened steel products and the heat-treating process. The current industrial standard technique for these measurements is micro-indentation, which is destructive and time consuming, and therefore not suitable for the need of industrial on-line volume inspection. There have been continuous efforts to search for new methods for evaluating hardness and case depth in a non-contact and non-destructive fashion. In recent years, photothermal techniques have shown strong potential for non-contact and remote hardness and case depth evaluation. A number of photothermal applications to hardness measurements in metals have been reported in the literature. Various independent research groups have reported a well-established anticorrelation between thermal diffusivity/thermal conductivity and microhardness. Jaarinen and Luukkala [1] made the first attempt to study the properties of surface hardness of steel in terms of an inverse process and developed a numerical technique based on the solution of the thermal-wave equation using a two-dimensional finite difference grid. Lan et al. [2] and Mandelis et al. [3,4], showed the capability of photoacoustic (PA) and photothermal radiometric (PTR) detection as depth profilometric techniques for case hardened steels using inverse-problem reconstruction algorithms. Both groups demonstrated anticorrelation between the case depth dependent microhardness and thermal conductivity/diffusivity of the material. Further PTR studies of hardness case depth profiling were carried out by Walther et al. [5], Fournier et al. [6] and Nicolaides et al. [7,8]. The last group also investigated the microstructure change and the physical mechanisms of the thermal diffusivity depth-profile generation for carburized and quenched AISI-8620 steels. They showed that the variation of thermal diffusivity with depth is dominated by the carbon concentration profile, while the absolute thermal diffusivity values are dominated by microstructural

*Corresponding author. Institute of Modern Optical Technologies, Suzhou University, 1 Shizi Street, Suzhou, Jiangsu Province 215006, PR China. Tel.: +86 512 65113356.
E-mail address: chinhua.wang@suda.edu.cn (C. Wang).

0963-8695/$ - see front matter © 2006 Elsevier Ltd. All rights reserved.
doi:10.1016/j.ndteint.2006.09.005

changes occurring during quenching. All those investigations have focused on samples heat-treated in the presence of carbon or nitrogen ambient, to form a concentration gradient which subsequently defines the hardness case depth profile after quenching. Recently, the PTR technique was also used in the characterization of non-diffusion controlled steel case depth: The hardness penetration depth of grind-hardened SAE 4140 steel using the calibration curve of case depth versus phase sum [9] and the effect of cooling rate on hardness and thermal diffusivity by means of water end-quenched heat treatment in a metallurgical Jominy bar made of AISI 1018 steel [10], were evaluated. As is well known, the PTR signal is sensitive to both thermophysical properties and sample geometry. To simplify geometry effects, all reports to-date concern laboratory based investigations, in which all samples were well defined, prepared and machined flat surfaces with a good finish. Recently, the evaluation of machined cylindrical samples was reported in order to demonstrate the feasibility of the PTR technique with non-flat geometries [11,12]. In those studies it was shown that thermal-wave interference occurs in layered curved samples and the details of the interferometric pattern are affected by the degree of curvature. Therefore, motivated by the potential of PTR for non-destructive testing of industrial steel products of different shapes toward quality control of volume production, this paper demonstrates, for the first time, the capabilities of the PTR technique in measuring the effective case depth in case-hardened industrial steels. Specifically, we evaluated three different types of industrial screws (all made of C1018 steels but with different geometries), heat treated and carburized with different case depths. Each type of geometry involved a group of several samples to account for the sample-to-sample variation due to the nature of case-hardened industrial products. Calibration curves for each type of screw were established statistically using the relationship between conventional mechanical indentation results and PTR interferometric phase minima. Well-resolved calibration curves were constructed and it was shown that it was possible to measure accurately and non-destructively the unknown effective case depth of sample groups of each type of screw, based on the established calibration curve for the given geometry.

2. Sample preparation and experiments

All the samples tested were made of C1018 steel (composition: 0.14–0.2%C, 0.6–0.9%Mn). Three types of screws with different screw heads (i.e., hexagonal with six flat surfaces, cylindrical and spherical heads) were evaluated. Fig. 1 shows the types of samples involved in this study. Two measurements were made on the heads of screws, on spots 1 and 2 for each screw shown in Fig. 1. There were 10 samples of each type of screw and each hardened case depth. Four nominal hardness case depths (0.01, 0.02, 0.03 and 0.04 in) were delivered by the heat-

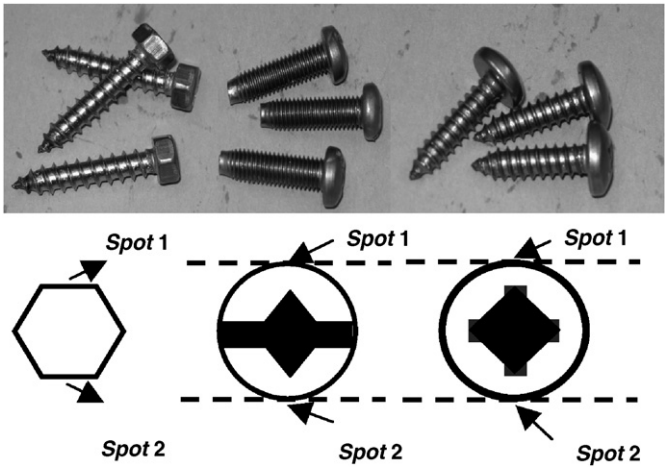

Fig. 1. Illustrations of the screw samples under test. From left to right: hexagonal, cylindrical, spherical. The lower part of the graph is the top view of the screw heads.

treating plant for each type of screw. The actual case depth was measured by a conventional indenter and was correlated to results from the PTR technique. All the samples underwent standard industrial carburizing heat treatments to obtain different case depths. For the same nominal case depth all three types of screws were grouped together to have exactly the same heat treatment, Table 1. After hardening, all the screws were tested using PTR frequency scans, and then subgroups of each type of case hardened screw were subjected to mechanical indentation measurements while the remaining screws were not indented and served as a reference group. The case depths of these latter screws were estimated using the calibration curves generated from the indented groups.

The experimental setup is shown in Fig. 2a. The optical source was a high-power semiconductor laser (Jenoptik, max. ~20 W). The output of the laser was modulated by a periodic current driver (high-power laser diode driver, Thor Labs), the frequency of which was controlled by the computer and also served as the lock-in reference. The beam was focused or expanded depending on the measurement scheme, and then impinged onto the surface of the sample with a spot size between 1 and 22 mm by adjusting the position of the converging lens. The measurement spot (spot 1 or spot 2 in Fig. 1) on the sample coincided with the focal point of one of the off-axis paraboloidal mirrors. The harmonically modulated infrared radiation from the sample surface was collected by the other off-axis paraboloidal mirror and detected by a HgCdTe detector (EG&G Judson Model J15016). The signal from the detector was amplified by a low-noise preamplifier (EG&G Judson PA101) and then fed into a lock-in amplifier (EG&G Instruments Model 7265) interfaced with a PC. The frequency scan from 2 Hz to 10 kHz generated thermal waves the diffusion length of which covered most of the case depths of industrial relevance. A total of 50 frequency data points were recorded for each

Table 1
Matrix of screw samples used for the generation of calibration curves using PTR and a mechanical indenter measurements

Sample type	Group	Frequency at phase minima (Hz) using focused beam (Dia.~1 mm)		Frequency at phase minima (Hz) using expanded beam (Dia.~22 mm)	
		Indenter tested	Untested	Indenter tested	Untested
$14-10\times1\frac{1}{4}$ (hex-head) 10 pcs for each group	Group 1 nominal-0.01″	—	—	369.0±40.9	366.6±61.8
	Group 2 nominal-0.02″	136.2±14.1	141.7±25.2	231.9±24.7	238.8±28.9
	Group 3 nominal-0.03″	54.5±5.1	58.9±9.9	175.3±7.6	183.6±20.9
	Group 4 nominal-0.04″	21.7±1.3	21.8±2.1	128.6±14.3	126.2±19.2
12 × 7/8 (spherical head) 10 pcs for each group	Group 1 nominal-0.01″	—	—	—	—
	Group 2 nominal-0.02″	25.1±6.5	20.2±3.7	137.3±13.8	138.5±10.4
	Group 3 nominal-0.03″	15.1±1.3	14.1±1.6	108.1±4.2	94.9±5.9
	Group 4 nominal-0.04″	10.6±1.0	9.5±1.0	58.9±6.2	54.1±8.1
10-24 × 7/8 (cylindrical head) 10 pcs for each group	Group 1 nominal-0.01″	—	—	—	—
	Group 2 nominal-0.02″	51.0±12.1	54.9±12.1	172.3±16.2	170.2±12.2
	Group 3 nominal-0.03″	25.2±3.0	28.0±4.5	114.1±12.8	113.4±13.6
	Group 4 nominal-0.04″	10.1±1.6	12.0±1.4	45.1±5.9	43.7±5.8

scan. Fig. 2b shows an alternate measurement modality using sine-swept excitation waveforms and cross-correlation signal analysis. While the experimental set-up and the optical path are the same as in Fig. 2a, the block surrounded by the dotted line in Fig. 2a is replaced by Fig. 2b. Details are described in Section 3.4. In the experiments, two beam profiles were employed to test the sensitivity of case depth probing to thermal-wave dimensionality, i.e., focused beam (Dia. ~1 mm) and expanded beam (Dia. ~22 mm). In order to eliminate the instrumental transfer function, a C1018 flat surface sample (Dia. ~20 mm) was used to normalize the sample signal in the form of the ratio of amplitudes and the difference of phases between sample and reference signals.

3. Results and discussion

3.1. PTR measurements

All samples were measured using either a focused beam or an expanded beam before and after the hardening process. Considering the usual variations in geometry, surface finish or surface color in industrial volume products, each sample was measured on two spots. Then all the measurement data for the same type of screw and the same hardness case depth were statistically processed in order to generate a meaningful calibration curve (or calibration band) for industrial applications. It should be noted that only the results of normalized PTR phase are meaningful, because the amplitude of the signal is sensitive to sample surface optical conditions and reflectivity changes which may produce artifacts. Phase signals, on the other hand, are independent of surface reflectivity and lead to pure thermal-wave measurements free of such artifacts [13]. Fig. 3 shows typical PTR phase measurement for cylindrical head screws before hardening using a focused and an expanded beam, respectively. The phase shape difference between focused and expanded beam, especially in the low frequency range, is due to the well-known dimensional effects of thermal-wave propagation [14]. The mean value and standard deviation in the plots were obtained based on a group of 10 samples and a total of 40 measurements from this group, Table 1. They serve as baseline values and as a reference for the measurements with hardened samples.

Figs. 4 and 5 show the PTR frequency scan for the hardened (nominally 0.03″ case depth) spherical-head screws using a focused beam and an expanded beam, respectively. In these plots, the upper part shows all frequency-scan traces obtained on the hardened samples. Both figures show consistency in shape and give a measure of natural variations from sample to sample. The largest variations are observed at the high frequency end, as expected [8], due to the surface roughness and the commensurably short thermal diffusion length which probes the randomly distributed intra-roughness region, thus producing substantial variation to the overall PTR phase. In the low frequency range, both phases exhibit interferometric phase minima between ca. 10 and 300 Hz, depending on the beam size. The phase minimum is more pronounced using the expanded beam measurement than that using the focused beam. The phase minima in the plots are the result of thermal-wave confinement (a diffusive standing wave) between substrate and surface hardened layer [12]. For a fixed overlayer thickness, in a manner analogous to freely propagating (rather than diffusing) wave fields, the height of the thermal-wave antinode depends on the difference in thermophysical properties between hardened layer and unhardened substrate. Furthermore, thicker upper layers result in antinodes of larger height, such as those shown for 0.01″ and 0.02″ nominal case depth in Fig. 6: The shallow antinode in

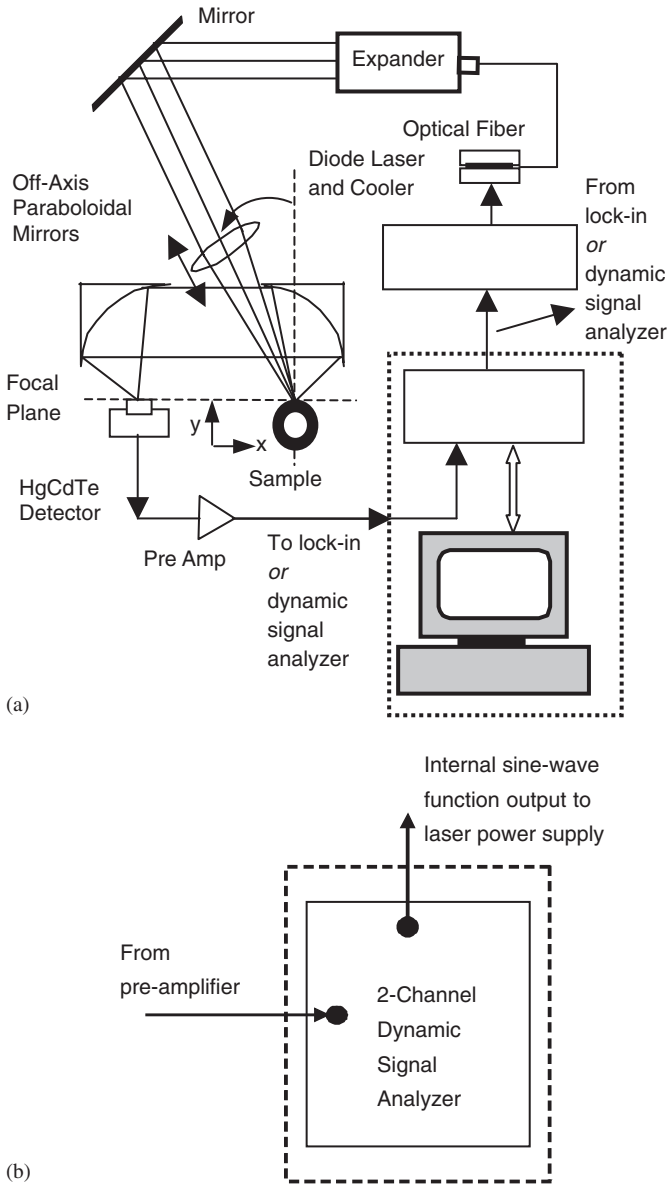

Fig. 2. Experimental setup for PTR measurements. (a) Lock-in point-by-point frequency-scan configuration. (b) SS wide-bandwidth configuration using a dynamic signal analyzer. The optical path is the same as that in Fig. 2a, but the block surrounded by dotted lines in Fig. 2a is replaced by Fig. 2b.

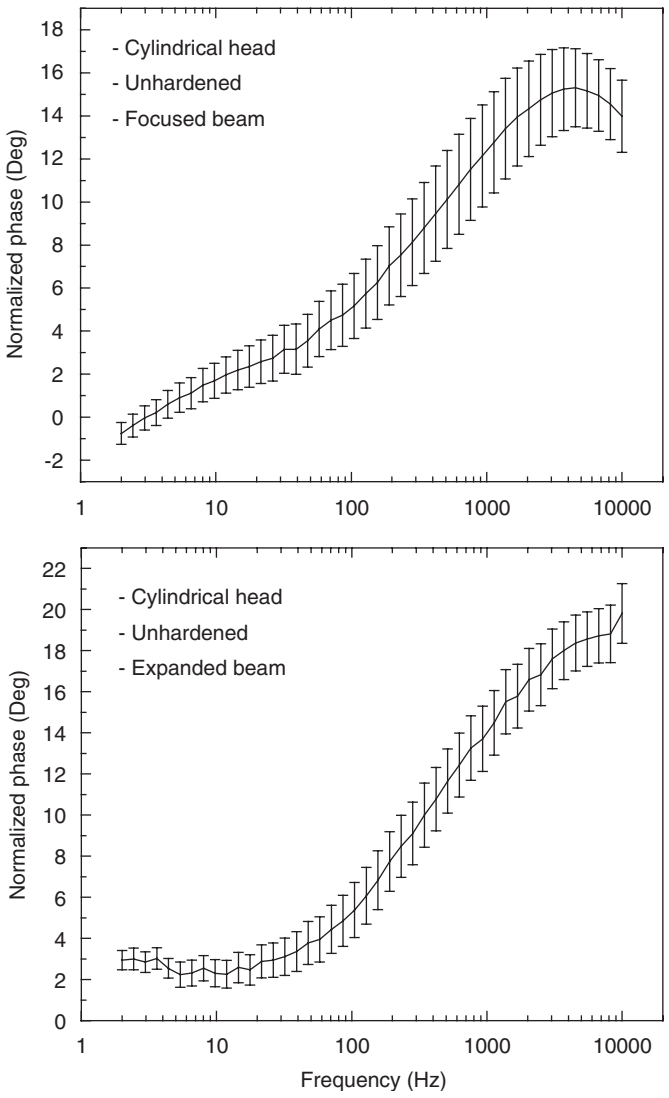

Fig. 3. Typical statistical PTR phase results for cylindrical-head screws before hardening using a focused (upper) and an expanded (lower) laser beam, respectively.

Fig. 6a corresponds to 0.01″ case depth, whereas the deeper antinode in Fig. 6b corresponds to 0.02″. In terms of dimensionality, a wide beam mostly generates one-dimensional (forward) thermal-wave confinement within the hardened region which is more sensitive to the actual hardness boundary (or gradient), whereas a focused beam results in significant thermal-wave signal contributions from all radial directions, thus diminishing the overall importance of the forward direction and of the case boundary. In some cases of shallow case depths (~0.01″), focusing the laser beam resulted in complete elimination of the phase minimum. Therefore, 0.01″ represents the minimum case depth detection limit using a focused laser beam. This is *not* a lower limit when a broad laser beam is used, as seen in Fig. 6a. Based on the fact that for these samples mechanical indenter results showed that the degree of surface hardness is independent of case depth, Fig. 7, the effective thermophysical property change (thermal diffusivity and conductivity) of the hardened layer does not depend on the thickness of the hardened layer. Therefore, the location of the phase minimum on the frequency axis can be employed to estimate the effective case depth of the hardened layer without further data correction to account for surface hardness variations. The frequency positions of the phase minima were located by a computational polynominal fitting (a seven-order polynominal is employed) and a minimum-finding algorithm which is done using a MATLAB program based on the zero value of the polynomial derivatives. Fig. 8 shows an example of polynominal fit to data from a nominally 0.03″ case depth hardened spherical-head screw using an expanded beam.

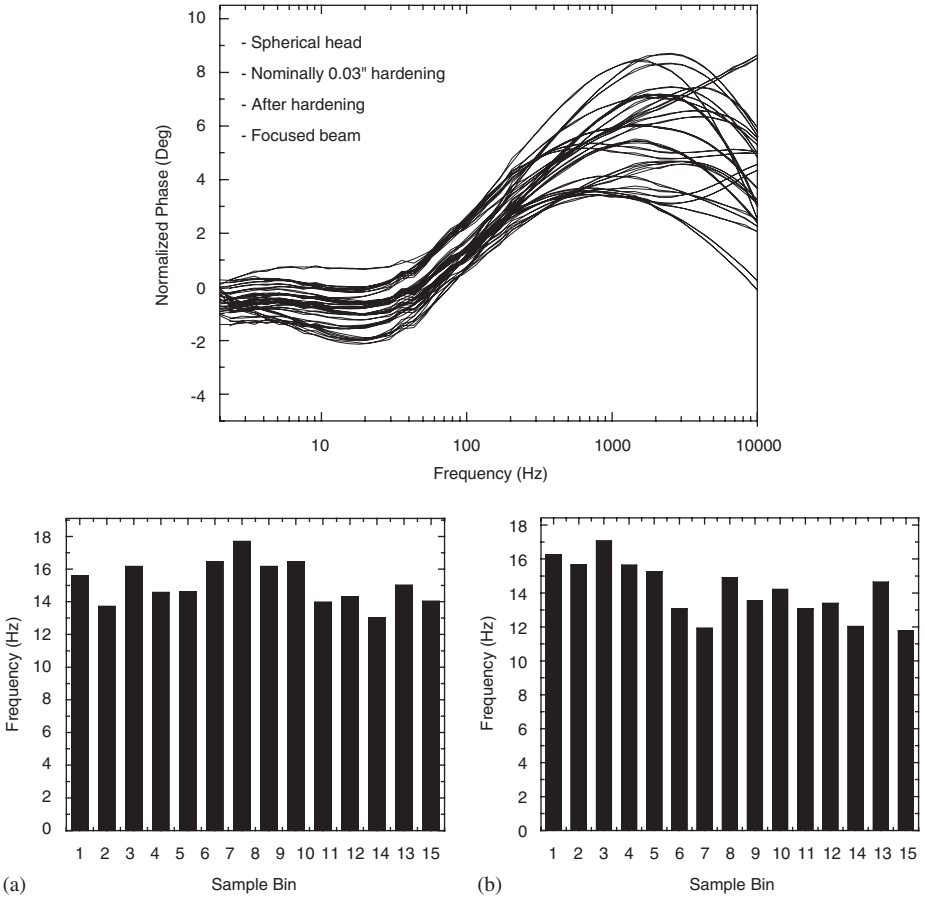

Fig. 4. PTR frequency scan of hardened (nominally 0.03″ case depth) spherical-head screws using a focused beam. Lower part (a): frequencies of phase minima vs. sample bin for samples subjected to a mechanical indentation case depth measurement and (b) frequencies of phase minima for samples untested by the mechanical indenter.

The fitted seventh-order polynominal is $y(f) = 3.11001 + 35.8927f - 61.75457f^2 + 43.79467f^3 - 17.60857f^4 + 4.43277f^5 - 0.65003f^6 + 0.04146f^7$, from which the zero value of the derivative was found to be at 107.5 Hz. The resulting phase minima frequency locations are plotted in the lower part of Figs. 4 and 5. For all hardened samples, a subset was chosen to undergo mechanical indentation tests in order to generate the calibration curve for the particular type of screw head geometry. The remaining samples were used as a reference group and were further compared with the mechanically tested group. The phase minima of the indentation tested and untested are shown in Figs. 4a, b and 5b, respectively. Typical statistical results from each plot are given in Table 1. It is seen that the minimum frequency spread for samples of the same group is ~10% and ~6–7% around the mean for focused beam and expanded beam, respectively. The results for other types of screws were obtained in the same manner (Table 1) and were correlated with the mechanical hardness test results.

3.2. Mechanical tests

Four samples of each type of screw were chosen for hardness case depth measurements using a conventional mechanical indentation method. The samples were cut into halves, encased in resin and the microhardness was measured from both edges toward the center. Fig. 7 shows typical mechanical (Rockwell, RC) hardness depth-profile test results for hexagonal head screws with nominal 0.03″ hardness case depth. It is seen that for nominally identially same hardness case depths, the variation of the hardness profile is significant, especially at large depths, although surface hardness values converge. To correct for the large baseline variations, the *effective case depth*, D_{eff}, was defined as

$$D_{\text{eff}} = H^{\text{RC}}_{\text{min}} + \frac{1}{e}(H^{\text{RC}}_{\text{max}} - H^{\text{RC}}_{\text{min}}). \quad (1)$$

The effective case depths calculated from Fig. 7(a) are shown in Fig. 7(b), from which the mean case depth and standard deviation were found to be: $\langle D_{\text{eff}} \rangle = 401.6 \pm 31.9\,\mu\text{m}$, representing a ~8–10% uncertainty (spread) for the hexagonal-head group of samples.

3.3. Correlations

Having measured the PTR phase minima and the mechanically tested hardness profiles for each type of

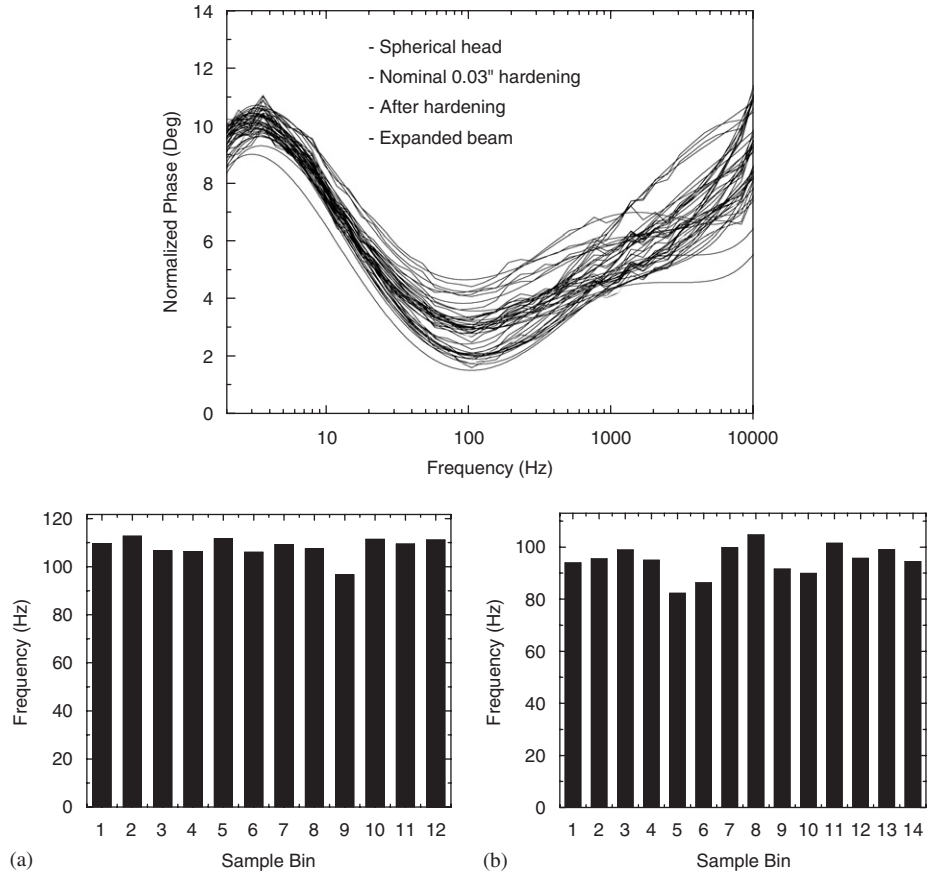

Fig. 5. PTR frequency scan of hardened (nominally 0.03″ case depth) spherical-head screws using an expanded beam. Lower part (a): frequencies of phase minima vs. sample bin for samples subjected to a mechanical indentation case depth measurement and (b) frequencies of phase minima for samples untested by the mechanical indenter.

screws, the correlation between the effective case depth and the phase minima was then established. Figs. 9–11 show these correlations in the form of calibration curves (or calibration bands, if the vertical and horizontal standard deviations are taken into account) for the hexagonal, cylindrical and spherical-head screws using a focused beam and an expanded beam. In the plots, mechanically tested and untested results are plotted separately to view the consistency between the two groups. Operationally, the results from the destructively indenter-tested samples were used to generate the calibration curve. This curve, along with the value of each phase-frequency minimum of the remaining unindented samples of a given head type, was used to estimate the effective case depth of the unidented sample in a non-destructive manner. It is clear that the two curves for all screw types and for both beam profiles share common features. The variances of the mechanical test results are similar to those of the PTR phase minima for all case depths larger than ca. 300 μm, implying comparable sample-to-sample variations. The larger distribution in PTR measurements for some shallow case depths is due to increased signal variance from sample to sample which impeded accurate determination of the phase minima from the frequency scan. The reason for that is that those phase minima occur at higher frequencies since the shallower case depth confines the thermal wave closer to the sample surface within the effective overlayer [14]. Phase minima located at high frequencies are affected by random surface roughness effects which tend to dominate the PTR spectrum at the high frequency end [8]. As discussed earlier on, when the case depth is very shallow, the effective thermophysical properties within the hardened layer can be greatly affected by surface roughness, yielding values controlled by a mixture of the roughness interspace gas (air), fractal heat conduction physics [15] and the possibly very different degree of hardness of the thin rough layer. All these complications may cause significant variation in the location of phase minima. In conclusion, the effective minimum case-depth detection limit for the C1018 steel screws using PTR phase minima was found to be ca. 300 μm. It is clear from Figs. 9–11 that when the focused- vs. expanded-beam correlation plots are compared, the expanded beam generates larger minimum phase-frequency shifts than the focused beam for the same case depth. Furthermore, for the shallowest case depths ($\leqslant$300 μm) the variances of the expanded beam correlation curves are smaller than those for the focused beam curves. These facts imply that expanded beam profiles have higher resolution

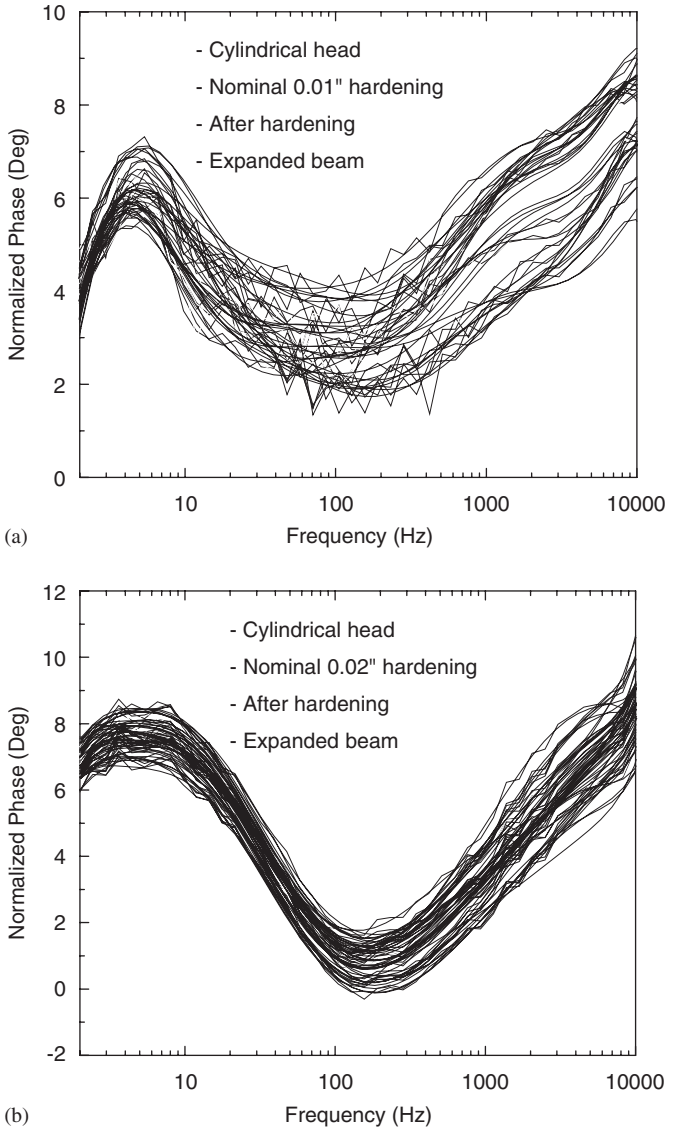

Fig. 6. PTR phase frequency scans of groups of cylindrical-head screws. Nominal case depth (a) 0.01″; (b) 0.02″. Laser beam size: 22 mm.

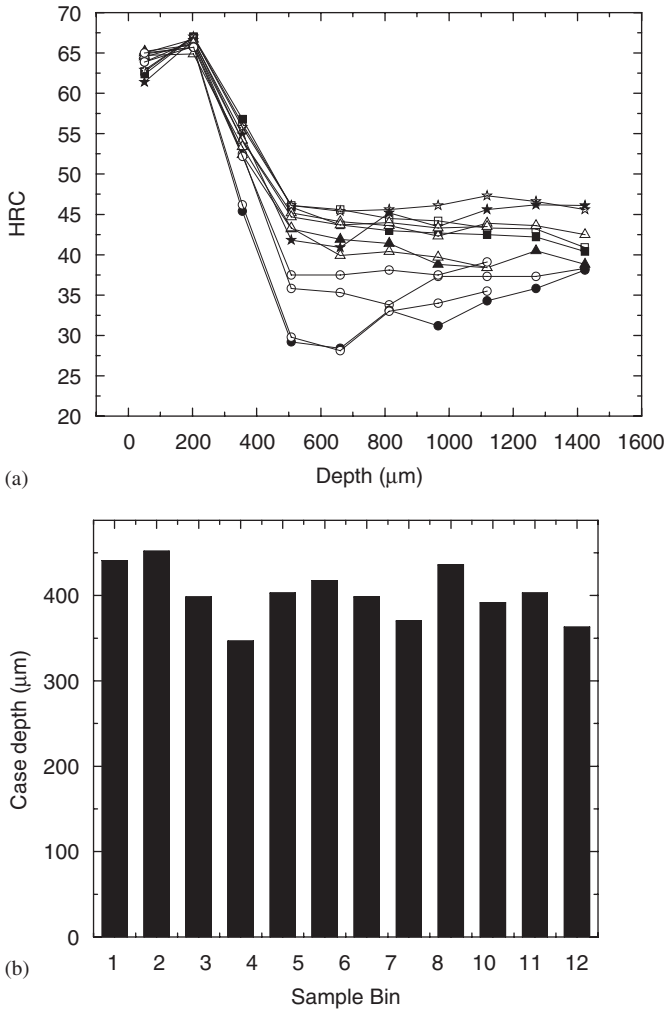

Fig. 7. Mechanical indentation hardness test results for nominally 0.03″ case depth hardened hexagonal head screws.

and dynamic range than focused beam profiles for all screw shapes and should be the preferred measurement modality.

3.4. Fast swept-sine measurement

The aforementioned lock-in amplifier (LIA) based experimental scheme usually yields high signal-to-noise ratio measurements, but measurements are of relatively long duration owing to the point-by-point nature of LIA signal acquisition character and the LIA time constants (~1 s) used in the experiments, especially at low frequencies. In our experiments, 50 frequency points were measured between 0.5 Hz and 10 kHz, and five measurements were taken at each frequency for averaging. Therefore, it took ~30 min to complete one scan. To speed up measurements toward industrial on-line applications, a fast swept-sine (SS) measurement scheme was introduced. This

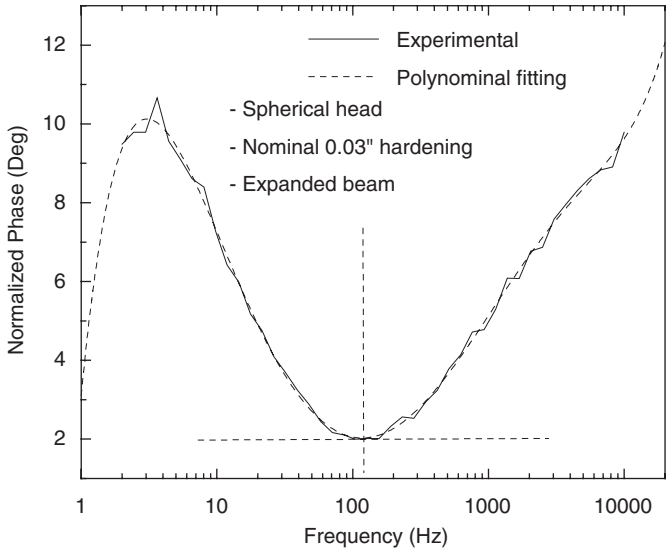

Fig. 8. Experimental data and their polynomial best fit for a spherical-head screw with a nominal 0.03″ case depth hardening using an expanded beam.

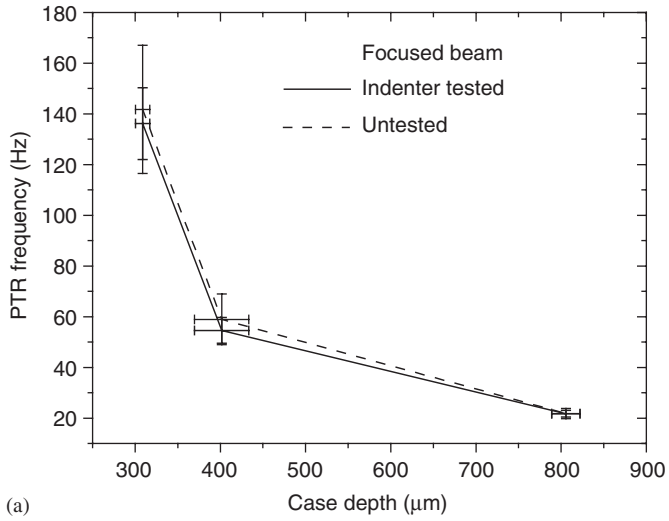

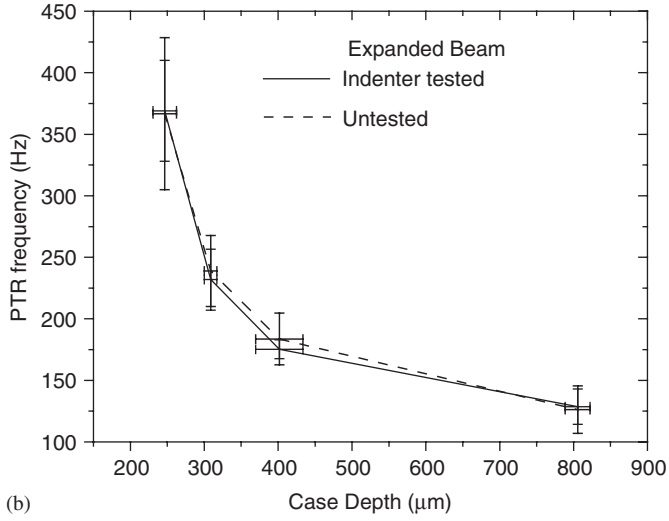

Fig. 9. Correlation between the PTR phase minima and the mechanically determined effective case depth for hexagonal-head screws using a focused beam (a) and an expanded beam (b).

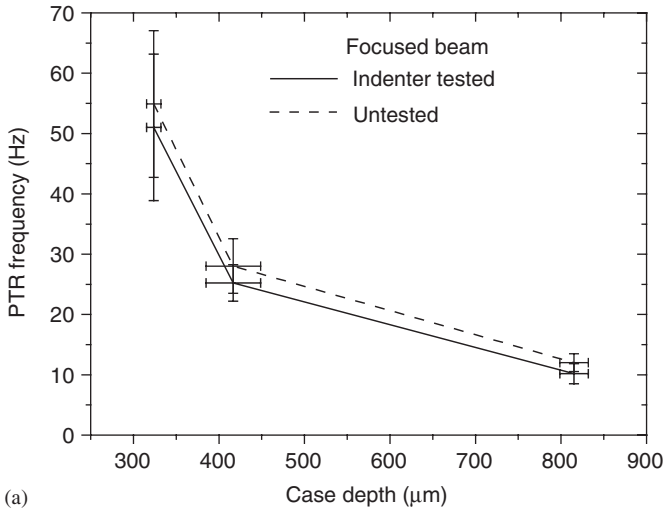

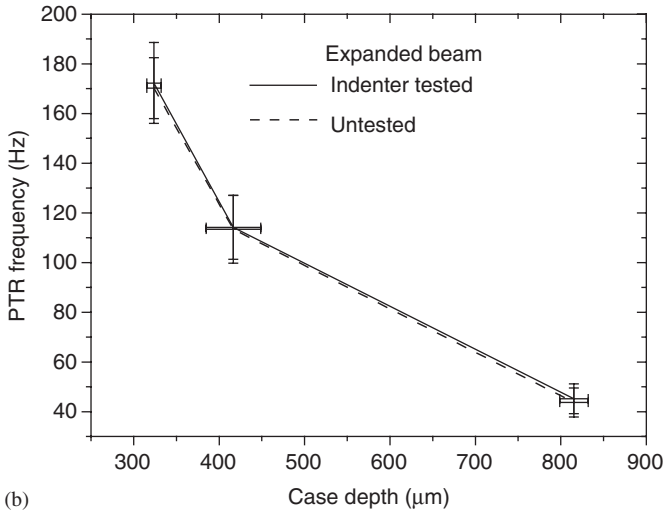

Fig. 10. Correlation between the PTR phase minima and the mechanically determined effective case depth for cylindrical-head screws using a focused beam (a) and an expanded beam (b).

measurement scheme employs a two-channel dynamic signal analyzer (Stanford Research Systems Model SR785), Fig. 2b, to fast generate a sine-wave signal with linearly swept frequency $f = f(t)$ which serves as a reference waveform as well as input to the current modulation of the diode laser. The analyzer cross-correlates the reference sine-wave signal and the PTR output signal from the detector and through spectral analysis it generates and outputs the amplitude and phase vs. frequency of the PTR signal in real time. In this measurement modality, if 44 points are measured between 2 Hz and 10 kHz and a 1-s time constant is chosen, it takes ~74 s for a complete frequency sweep. Comparisons of the measurement quality using a conventional LIA and sine sweeps of various durations are shown in Fig. 12. The measurements were made on a cylindrical-head screw sample. Phase normalization for the LIA and the SS measurements were made, respectively, using the LIA and SS phase measurements from a flat surface of an unhardened thermally thick C1018 steel sample. In the SS measurements, three different time constants (1.5, 1.0 and 0.75 s), which correspond to total measurement times of 112, 74 and 58 s, respectively, were used to compare signal quality. It is seen in Fig. 12 that all the curves are similar in shape attesting to the reliability of all the measurements. The difference between lock-in and SS measurement at low frequencies is due to the long time constant (>2 s) used in the lock-in measurements resulting in long-time averaging and slow response. It can be seen that the quality of LIA and SS measurements is comparable. Detailed signal examination reveals that the worst quality is encountered in SS 58-s measurements, which is understandable since the shortest scan-time implies the least photothermal excitation energy input to the system. For time constants greater than 58 s (i.e., 74 and 112 s), the measurement quality is equivalent to that of using a LIA, but with significantly shorter time, which

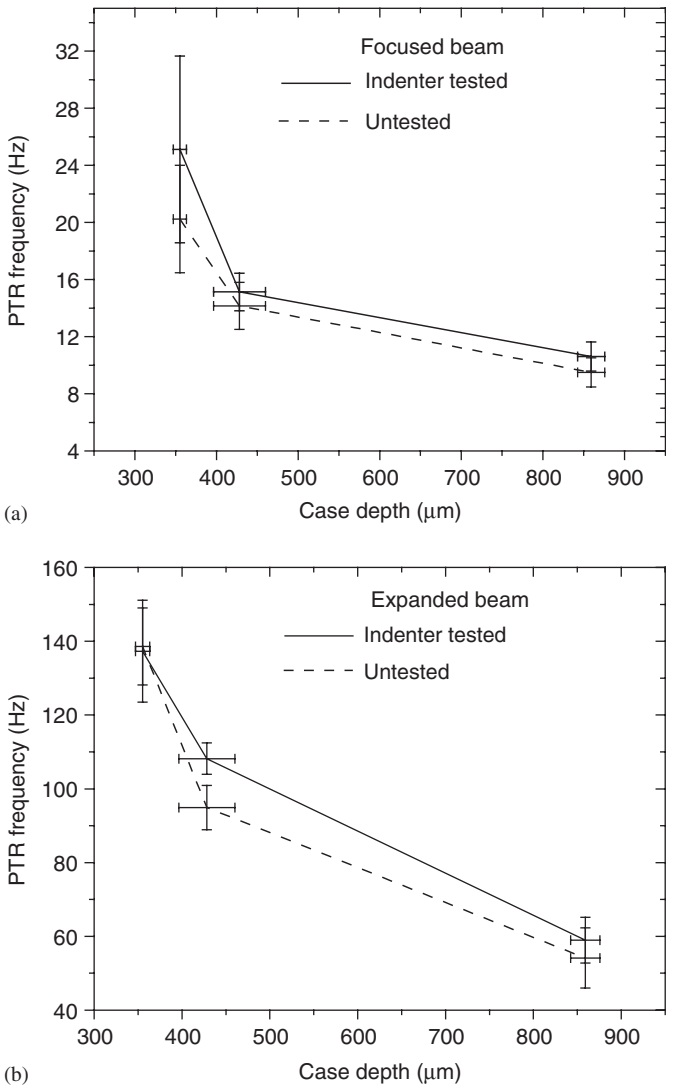

Fig. 11. Correlation between the PTR phase minima and the mechanically determined effective case depth for spherical-head screws using a focused beam (a) and an expanded beam (b).

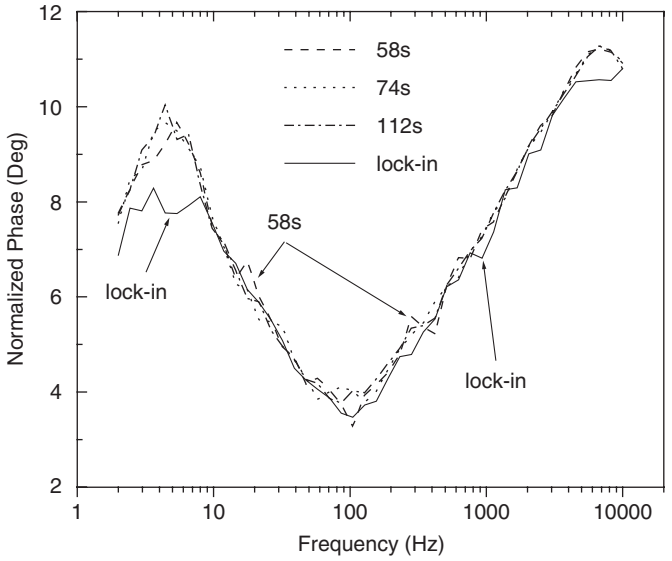

Fig. 12. PTR signal quality comparison of a conventional LIA and a swept-sine (SS) measurement using a cylindrical-head screw sample.

makes the technique acceptable for practical industrial applications.

4. Conclusions

We have demonstrated a quantitative non-destructive technique for evaluating effective case depth in heat treated case-hardened steel products using laser PTR phase minima. Several types of heat-treated C1018 industrial steel screws (hexagonal, cylindrical and spherical heads) were statistically evaluated and correlation/calibration curves for each type of sample were established using conventional destructive indentation measurements to extract actual hardness case depths. It was found that the PTR thermal-wave interferometric phase minimum determination method is suitable for evaluating case depths $\geqslant 300\,\mu m$ in this type of steel. The expanded beam measurement scheme generates higher resolution and higher dynamic range than the focused beam scheme. It was shown that PTR thermal-wave interferometric phase-frequency minima coupled with SS waveforms and signal cross-correlation and spectral analysis can be used as a fast on-line inspection method of industrial steel products for quality control of industrial heat treating processes.

Acknowledgements

The support of Materials and Manufacturing Ontario (MMO) is gratefully acknowledged. The authors are grateful to Steve Dong and Sushil Suri of Metex Heat Treating for their help with providing and hardening the screw samples as well as for performing mechanical indentation tests.

References

[1] Jaarinen J, Luukkala M. Numerical analysis of thermal waves in stratified media for non-destructive testing purposes. J Phys (Paris) 1983;44:C6–C503.
[2] Lan TTN, Walther HG, Goch G, Schmitz B. Experimental results of photothermal microstructural depth profiling. J Appl Phys 1995;78:4108–11.
[3] Munidasa M, Funak F, Mandelis A. Application of a generalized methodology for quantitative thermal diffusivity depth profile reconstruction in manufactured inhomogeneous steel-based materials. J Appl Phys 1998;83:3495–8.
[4] Ma TC, Munidasa M, Mandelis A. Photoacoustic frequency domain depth profilometry of surface layer inhomogeneities: application to laser processed steels. J Appl Phys 1992;71:6029–35.
[5] Walther HG, Fournier D, Krapez JC, Luukkala M, Schmitz B, Sibilia C, et al. Phorothermal steel hardness measurements-results and perspectives. Anal Sci 2001;17:s165–8.

[6] Fournier D, Roger JP, Bellouati A, Boue C, Stamm H, Lakestani F. Correlation between hardness and thermal diffusivity. Anal Sci 2001;17:s158–60.
[7] Nicolaides L, Mandelis A, Beingessner. Physical mechanism of thermal-diffusivity depth-profile generation in a hardened low-alloy Mn, Si, Cr, Mo steel reconstructed by photothermal radiometry. J Appl Phys 2001;89:7879–84.
[8] Nicolaides L, Mandelis A. Methods for surface roughness elimination from thermal-wave frequency scans in thermally inhomogeneous solids. J Appl Phys 2001;90:1255–65.
[9] Prekel H, Ament Ch, Goch G. Photothermal characterization of grinded-hardened steel. Rev Sci Inst 2003;74:670–2.
[10] Liu Y, Baddour N, Mandelis A, Wang CH. Inspection of an end quenched 0.15%–0.2%C,0.6%–0.9% Mn steel jominy bar with photothermal radiometry techniques. J Appl Phys 2004;96:1929–33.
[11] Wang CH, Mandelis A, Liu Y. Photothermal radiometry with cylindrical samples. J Appl Phys 2004;96:3756–62.
[12] Wang CH, Mandelis A, Liu Y. Thermal-wave nondestructive evaluation of cylindrical composite structures using frequency-domain photothermal radiometry. J Appl Phys 2005;97: 014911.
[13] Liu Y, Baddour N, Mandelis A. Transverse depth-profilometric hardness photothermal phase imaging of heat treated steels. J Appl Phys 2003;94:5543–8.
[14] Mandelis A. Diffusion-wave fields. Mathematical methods and green functions. New York: Springer; 2001.
[15] Boccara AC, Fournier D. Heat diffusion and fractals: heterogeneous media and rough surfaces. In: Hess P, Pelzl J, editors. Photoacoustic and photothermal phenomena, optical sciences, Vol. 58. New York: Springer; 1988. p. 302.